A new hybrid method for the analysis of surrounded antennas mounted on large platforms

Benoît Le Lepvrier, Renaud Loison, Raphaël Gillard, Philippe Pouliguen, Patrick Potier, Laurent Patier

A new hybrid method for the analysis of surrounded antennas mounted on large platforms

Benoit Le Lepvrier, Renaud Loison, Raphael Gillard, *Member, IEEE*, Philippe Pouliguen, Patrick Potier, and Laurent Patier

***Abstract*—An efficient technique to provide fast and accurate analysis of wide-band surrounded antennas mounted on electrically large platforms is presented and validated in this paper. The hybrid method combines Dual-Grid FDTD (DG-FDTD) with Iterative Physical Optics (IPO) to analyze on-platform antenna radiation. In section IV of this paper, DG-FDTD/IPO is applied to the analysis of a wide-band antenna mounted on a vehicle. The ability to address the problem of antenna placement is also demonstrated.**

***Index Terms*—hybrid methods, DG-FDTD, IPO, multi-scale method, antenna on structure.**

I. Introduction

ANTENNA placement on platforms such as aircraft, spacecraft or motor vehicles is becoming ever more constrained. Therefore, antennas are frequently placed close to complex elements on the structure. For this kind of problem, the complex vicinity of the antenna and the platform may have a significant effect on its behavior. So, it is of great interest to develop appropriate methods to estimate the distortion of the performance of the on-board antennas [1].

EM analysis of modern antenna-on-platform problems is very challenging for several reasons. Fig. 1 depicts the different regions which have to be considered when analyzing such problems. Obviously, the transmitting antenna (subdomain A) has to be simulated rigorously with a very fine mesh. Likewise, a potentially large subdomain including all complex elements in the vicinity of the antenna (subdomain B) must also be considered rigorously with a fine mesh. Although this caution requires large computational resources, it is necessary to correctly take into account the strong interactions between the transmitting antenna and the complex elements in its vicinity. The computational burden is compounded by the simulation of the platform (subdomain C), which represents a very large object electrically. The last challenge deals with the wide-frequency band over which antennas usually have to be analysed nowadays. This is mainly due to the evolution of applications toward increased bandwidth and frequency reconfigurability.

B. Le Lepvrier, R. Loison, and R. Gillard are with the European University of Brittany, France, INSA, IETR, UMR 6164, F-35708 Rennes, France (e-mail:Benoit.le-lepvrier@insa-rennes.fr; Renaud.Loison@insa-rennes.fr; Raphael.Gillard@insa-rennes.fr).

P. Pouliguen is with the Direction Générale de l'Armement / Direction de la Stratégie / Mission pour la Recherche et l'Innovation Scientifique (DGA/DS/MRIS), 92221 Bagneux, France (e-mail: philippe.pouliguen@dga.defense.gouv.fr).

P. Potier is with the Direction Générale de l'Armement (DGA), 35174 Bruz cedex, France (e-mail: patrick.potier@dga.defense.gouv.fr).

L. Patier is with the Centre National d'Etudes Spatiales (CNES), Toulouse 31401, France (e-mail: laurent.patier@cnes.fr).

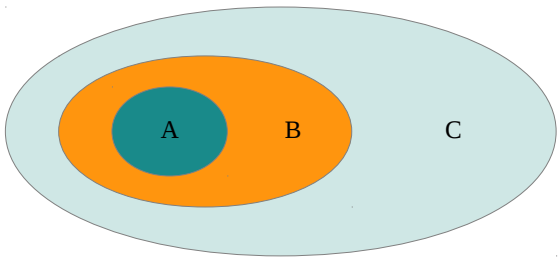

Fig. 1. A: Transmitting antenna, B: complex antenna vicinity, C: large supporting platform without any complex details.

With improvements in numerical techniques and computer performance over recent decades, direct Full Wave Methods (FWM) such as FDTD, FEM or MoM have appeared in the computation of antenna-platform problems. For example, in [2], [3], full wave time domain methods are used with parallelization schemes to perform the computation. These approaches have the great benefit of giving exact solutions. However, the necessity to finely mesh a complex and potentially large subdomain around the antenna and to simulate an electrically very large structure (platform) still require massive computational resources. Finally, regarding the problem illustrated in Fig. 1, direct FWM are properly suited for the subdomain A.

More efficient approaches, based on advanced FWM, have been proposed to analyze antenna-on-platform problems. For example, in [4], [5], the authors use Domain Decomposition Methods (DDM) with frequency domain solvers, decomposing the entire problem into several subregions. Subsequently, each of the subregions is analyzed separately and an iteration process is then started, whose aim is to link the different subregions. DDM based methods working in the time domain have also been proposed. For example, in [6] the authors use the FDTD method to analyze each independent subregion of the EM problem. Advanced FWM also include multi-scale methods, among which the Multi-Level Fast Multipole Method (MLFMM) is probably the most popular. For example, in [7], [8], MLFMM is applied to the Method of Moments (MoM) to analyze antennas mounted on aircraft. Time-domain multi-scale methods, such as the Dual-Grid FDTD (DG-FDTD) [9], have also been proposed to analyze problems presented by antennas on platforms, especially when wide-band characterizations are required. Finally, all the advanced approaches cited above allow rigorous and efficient simulation of subdomains

A and B. Although more efficient than direct FWM, advanced FWM do not completely succeed in cutting the computational burden, especially when very large platforms must be considered (such as domain C).

The most efficient way to deal with such large structures is certainly to use Asymptotic Methods (AM) such as Physical-Optics (PO) or Uniform Theory of Diffraction (UTD) [10], [11]. However, regarding the problem illustrated in Fig. 1, these methods are not properly suited for subdomains A and B.

Hybrid method coupling a direct FWM with an AM has frequently been written about in published material [12]–[22], however, this hybridization scheme does not give a satisfactory answer to our problem. Indeed, the complex antenna vicinity is both too complex to be analyzed with AM and too large to be computed efficiently with direct FWM.

As a consequence, a judicious solution consists of hybridizing an advanced FWM with an AM. One example of hybridization in the frequency domain is given in [23]. The authors use the FE-BI method, enhanced with domain decomposition and fast algorithms, to efficiently compute large antenna arrays. The platform is then analyzed with UTD or Iterative Physical Optics (IPO). But full frequency domain hybrid methods, such as the latter, are not appropriate for wide-band characterizations: thus time-domain methods have to be preferred. However, full time-domain hybrid methods experience difficulties in handling electrically large structures. In [20], a specific algorithm is proposed to improve efficiency and reduce memory storage in computation, but it has only been applied to small structures.

Hence, we propose here a new hybrid method combining a time-domain AFWM, DG-FDTD [9], and a frequency-domain AM, IPO [24]–[29]. DG-FDTD is a multi-scale time domain method based on FDTD which enables efficient and rigorous wide-band simulations of antennas and their complex vicinity [30]. The hybridization with IPO allows the limitation on the size of the structure to be overcome. In other words, the application domain of the DG-FDTD is extended to the accurate and efficient computation of surrounded antennas mounted on electrically large structures thanks to its combination with the IPO method. To our best knowledge it is the first time that DG-FDTD has been hybridized with IPO.

This paper is organised as follows. DG-FDTD/IPO is presented in section II. Section III is dedicated to the validation of the method. Examples of its application and associated numerical results are presented in Section IV. Finally, conclusions are drawn in the last section.

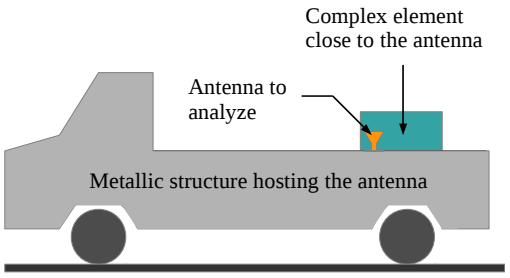

Fig. 2. Antenna mounted on a vehicle.

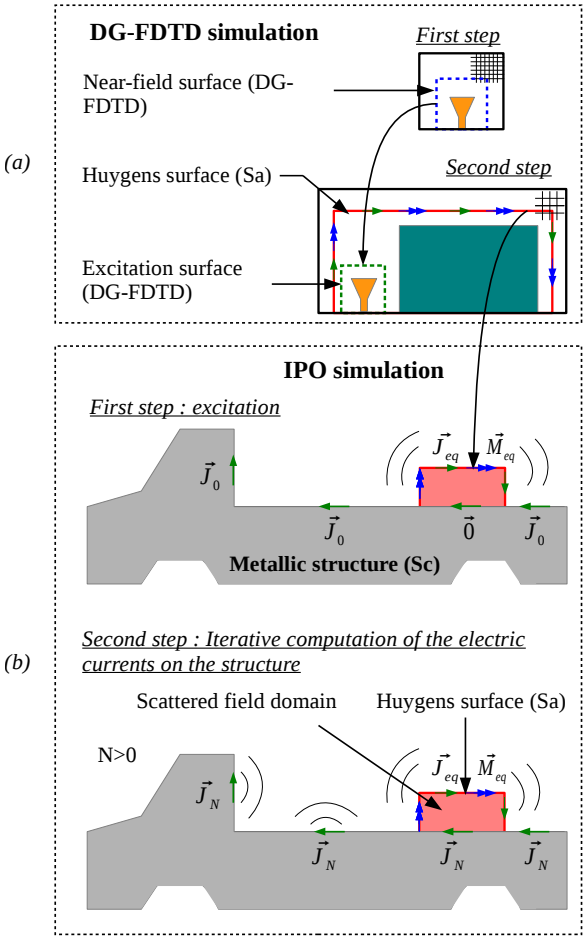

Fig. 3. DG-FDTD/IPO principle.

II. DG-FDTD/IPO FORMULATION

Let us consider the problem described in Fig. 2 in order to illustrate the DG-FDTD/IPO principle. The figure presents a basic configuration of a surrounded antenna which is mounted on a large metallic platform. More precisely, the antenna is placed close to a complex element (involving fine details) and mounted on a vehicle. The DG-FDTD/IPO approach consists in breaking down the initial EM problem into two successive simulations (Fig. 3). First, the DG-FDTD method is used to analyze the antenna and its complex vicinity rigorously and efficiently. Then, an IPO simulation of the metallic structure hosting the antenna is performed. DG-FDTD and IPO simulations are respectively described in sections II-A and II-C, whereas the hybridization technique is discussed in II-B.

A. DG-FDTD simulation

As mentioned above, DG-FDTD is a multi-scale time domain method based on FDTD which enables efficient and rigorous wide-band simulations of antennas and their complex

vicinity. Unfortunately, this method becomes inapropriate for the simulation of electrically very large structures due to the amount of resources needed. Only a brief description of the DG-FDTD principle is given here. For further details, please refer to the full description given in [9].

The DG-FDTD simulation of the antenna and its complex vicinity is performed using two FDTD simulations, which are run sequentially (Fig. 3 *(a)*). The objective of the first FDTD simulation (first step) is to very accurately characterize the isolated antenna. So, a very fine FDTD mesh can be used during this simulation and the FDTD volume is terminated by Absorbing Boundary Conditions (ABCs) in order to simulate an infinite problem. More precisely, in the general case presented in Fig. 3 *(a)*, five faces of this volume are terminated by perfectly matched layers, whereas a metallic boundary condition is applied on the sixth one (bottom face) to account for the ground plane. A near field surface is placed around the antenna in order to accurately store the primary radiation of the isolated antenna. In the second FDTD simulation (second step), the antenna and its vicinity are described using a coarser FDTD mesh. The primary radiation stored in the previous step is used as the excitation. ABCs are used again to simulate an infinite problem.

B. Interfacing of the DG-FDTD and IPO simulations

The hybrid DG-FDTD/IPO approach uses the surface equivalence principle [31] to interface DG-FDTD and IPO. Time domain equivalent currents representing the antenna and its vicinity are first derived from the DG-FDTD simulation. After a conversion in the frequency domain, these currents serve as excitation for the IPO simulation. Note that a time domain version of IPO also exists [27] but it has not been used here as it experiences difficulties in handling large structures.

More precisely, during the second DG-FDTD step, the tangential fields over a closed Huygens surface, including the antenna and its vicinity, are stored (Fig. 3 *(a)*). Then, Fast Fourier Transform (FFT) is applied to calculate the time harmonic tangential fields for any point within the DG-FDTD excitation spectrum. Note that two compression techniques are applied to interface the DG-FDTD simulation with the IPO code more efficiently. First, the number of time domain field samples on the Huygens surface is reduced according to the Nyquist sampling theorem. This time domain compression allows a reduction of the FFT burden, which enables faster calculation of the time harmonic form of the tangential fields. The second aspect of the compression deals with the reduction of the number of equivalent sources on the Huygens surface. With this objective, subapertures grouping several FDTD cells are defined and averaged tangential field components are calculated (linear interpolation). The equivalent sources $\vec{J_{eq}}$ and $\vec{M_{eq}}$ are finally obtained thanks to the equivalence principle formulas.

Next, a Huygens surface with the same location and dimensions as the one used in the DG-FDTD simulation is defined in the IPO simulation (Fig. 3 *(b)*). It is worth mentioning that the elements analyzed during the DG-FDTD simulation are not redescribed in the IPO simulation. As a consequence, the volume defined by the equivalent surface and closed by a flat metallic plate is empty. Finally, the equivalent currents calculated previously are positioned on this virtual surface. They will be used later as excitation for the IPO simulation.

C. IPO simulation

IPO [24]–[29] is an asymptotic method which consists of an iterative resolution of the Magnetic Field Integral Equation (MFIE). This method is used here to compute the currents over the metallic structure hosting the antenna. IPO is given preference over the traditional PO because it provides more accurate results when the shape of the metallic structures causes multiple reflections [32]. The IPO computation of the EM field radiated by the antenna on its platform is divided into 3 steps.

Firstly, IPO simulation starts by the computation of the magnetic fields $\vec{H^{S_a}_{S_c}}$, on the structure (S_c), radiated by equivalent currents $\vec{J_{eq}}$ and $\vec{M_{eq}}$ over the Huygens surface (S_a) (Fig. 3 *(b)*). This first step represents the excitation phase of the IPO simulation: excitation technique used here is based on the total-field/scattered-field decomposition principle. As indicated in Fig. 3 *(b)*, the Huygens surface plays the role of a frontier between the total-field and the scattered-field domain. Following this excitation principle, the equivalent currents do not radiate in the scattered field domain. For the rest of the structure (e.g. in the total field domain) the magnetic field $\vec{H^{S_a}_{S_c}}$ is computed using the Kirchhoff approximation:

$$\vec{H^{S_a}_{S_c}}(\vec{r_c}) = \int_{S_a} \vec{J_{eq}}(\vec{r_a}') \times \vec{\nabla}' G(\vec{r_c} - \vec{r_a}') \mathrm{d}S'_a + \frac{1}{jkZ_0} \times \vec{\nabla} \int_{S_a} \vec{M_{eq}}(\vec{r_a}') \times \vec{\nabla}' G(\vec{r_c} - \vec{r_a}') \mathrm{d}S'_a \quad (1)$$

where $\vec{r_a}'$ and $\vec{r_c}$ refer respectively to points over the equivalent Huygens surface S_a and over the structure S_c outside the Huygens surface. $\vec{\nabla}' G$ is the gradient of the free-space Green's function. The prime on the gradient operator indicates that the differentiation is performed on the source coordinates. Z_0 is the free space impedance and k is the wavenumber. The electric currents $\vec{J_0}(\vec{r_c})$ on the structure S_c after the excitation phase are given by

$$\vec{J_0}(\vec{r_c}) = 2\vec{n} \times \vec{H^{S_a}_{S_c}}(\vec{r_c}) \quad (2)$$

where $\vec{n}$ is the unit vector normal to the surface Sc at the point $\vec{r_c}$. Note that, because of the total-field/scattered-field decomposition principle, $\vec{J_0}(\vec{r_c})$ is equal to $\vec{0}$ for $\vec{r_c}$ in the scattered field area.

The second step of the IPO simulation consists of an iterative computation of the electric currents on the structure. These currents are induced by the radiation of both equivalent currents over the Huygens surface and currents on the other facets of the structure. The electric current $\vec{J_N}(\vec{r_c})$ at a point $\vec{r_c}$ at iteration N ($N > 0$) is given by

$$\vec{J_N}(\vec{r_c}) = \vec{J_0}(\vec{r_c}) + 2\vec{n} \times \int_{S_c} \vec{J}_{N-1}(\vec{r_c}') \times \vec{\nabla}' G(\vec{r_c} - \vec{r_c}') \mathrm{d}S'_c \quad (3)$$

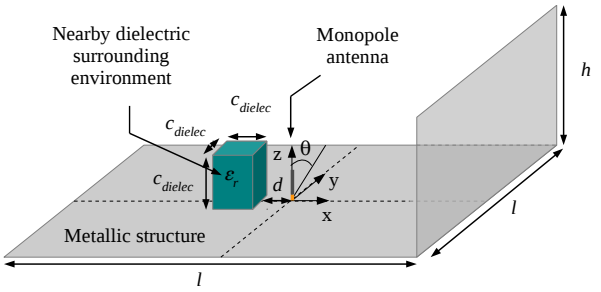

Fig. 4. Antenna mounted on a metallic structure. l = 3.9 m = 13 λ_{1GHz}, h = 1.15 m = 3.83 λ_{1GHz}, d = 0.15 m = 0.5 λ_{1GHz}, C_{dielec} = 0.18 m = 0.6 λ_{1GHz}, ϵ_r = 10.

where $\vec{r_c}$ and $\vec{r_c}'$ are two points on the structure S_c. Note that point $\vec{r_c}$ can belong to the scattered field domain since $N > 0$. This iterative process is repeated until a stable value for the electric currents is reached. It is worth noting that an IPO simulation with 0 IPO iteration ($N = 0$) corresponds to the traditional PO simulation. Consequently, $\vec{J_0}(\vec{r_c})$ are equal to the traditional PO currents.

The integrations presented in equations (1) and (3) are performed taking into account shadowing effects. For instance, in equation (1), if point $\vec{r_c}$ is not visible from point $\vec{r_a}'$, the contribution from point $\vec{r_a}'$ is set to zero.

The last step aims at computing the far field radiated at observation point $\vec{r}$ by the equivalent currents, and the currents on the structure. The Kirchhoff approximation is used again :

$$\vec{H}(\vec{r}) = \int_{S_a} \vec{J_{eq}}(\vec{r_a}') \times \vec{\nabla}' G(\vec{r} - \vec{r_a}') \mathrm{d}S_a' + \frac{1}{jkZ_0} \times \vec{\nabla} \int_{S_a} \vec{M_{eq}}(\vec{r_a}') \times \vec{\nabla}' G(\vec{r} - \vec{r_a}') \mathrm{d}S_a' + \int_{S_c} \vec{J_N}(\vec{r_c}') \times \vec{\nabla}' G(\vec{r} - \vec{r_c}') \mathrm{d}S_c' \quad (4)$$

$$\vec{E}(\vec{r}) = \frac{1}{jkY_0} \times \vec{\nabla} \int_{S_a} \vec{J_{eq}}(\vec{r_a}') \times \vec{\nabla}' G(\vec{r} - \vec{r_a}') \mathrm{d}S_a' + \frac{1}{jkY_0} \times \vec{\nabla} \int_{S_c} \vec{J_N}(\vec{r_c}') \times \vec{\nabla}' G(\vec{r} - \vec{r_c}') \mathrm{d}S_c' - \int_{S_a} \vec{M_{eq}}(\vec{r_a}') \times \vec{\nabla}' G(\vec{r} - \vec{r_a}') \mathrm{d}S_a' \quad (5)$$

where Y_0 is equal to $1/Z_0$.

III. Validation of DG-FDTD/IPO

This section is dedicated to the validation of the DG-FDTD/IPO approach presented in section II. To do so, the radiation of a canonical antenna-on-structure is computed with both DG-FDTD/IPO and advanced FWMs.

A. Description of the validation scenario

The EM problem (Fig. 4) includes a monopole antenna surrounded by a dielectric element, mounted on an electrically large metallic structure. The monopole antenna, whose central frequency is 1 GHz, is placed at the center of a rectangular finite ground plane. Moreover, a vertical metallic plate loads this ground plane so as to create a dihedral structure. Finally, a lossless dielectric cube is placed close to the monopole in order to create a scenario requiring a rigorous description of the antenna and its vicinity.

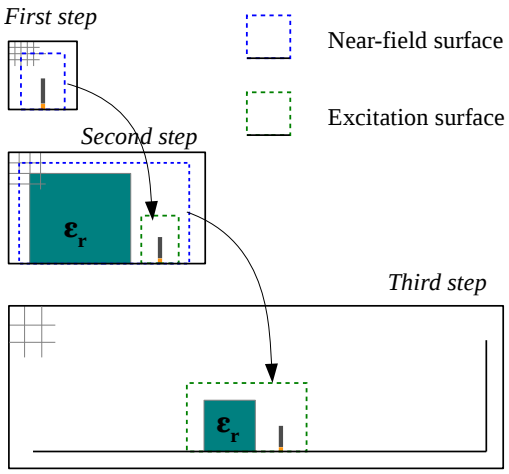

Fig. 5. Multi-Level DG-FDTD computation of the validation scenario.

It must be noted that the dimensions of this scenario are smaller than the ones encountered in real antenna-on-platform problems. This choice is justified by the need to get, in a reasonable amount of time, full wave computation of the overall problem as a reference.

B. Reference simulations

The complete validation scenario is first computed with two multi-scale approaches: MLFMM and Multi-Level DG-FDTD (ML DG-FDTD) [33]. Note that these two approaches are based on rigorous methods (respectively MoM and FDTD). They allow multi-scale problems such as the validation test case to be computed both rigorously and efficiently. Moreover, the use of a time-domain volume method (ML DG-FDTD) and a frequency-domain surface method (MLFMM), increases the reliability of the validation.

MLFMM computation is performed with FEKO [34] software using a $\lambda_{1GHz}/12$ standard mesh to describe the elements (146,537 triangles). MLFMM is combined with the Surface Equivalence Principle (SEP) to analyze the dielectric region close to the antenna.

As mentioned above, the validation scenario was also simulated with Multi-Level DG-FDTD. This method is an extension of DG-FDTD where the number of successive FDTD steps is not limited to two (as is the case in Fig. 3 *(b)*). This time domain multi-scale method is well suited to the simulation of highly multi-scale EM problems. Here, the simulation of the overall scenario is broken down into three FDTD simulations (Fig. 5). The first step, aiming at precisely simulating the monopole, uses a uniform $\lambda_{1GHz}/60$ cubic mesh, which results in an FDTD volume of $60 \times 60 \times 56$ unit cells. Then, the antenna and the dielectric block are analyzed using a coarser

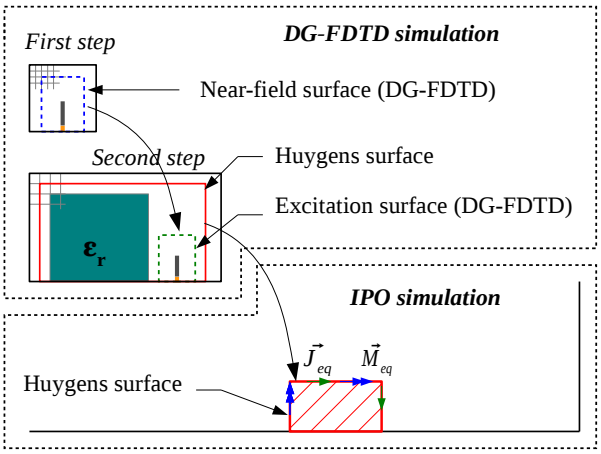

Fig. 6. DG-FDTD/IPO breakdown of the validation structure.

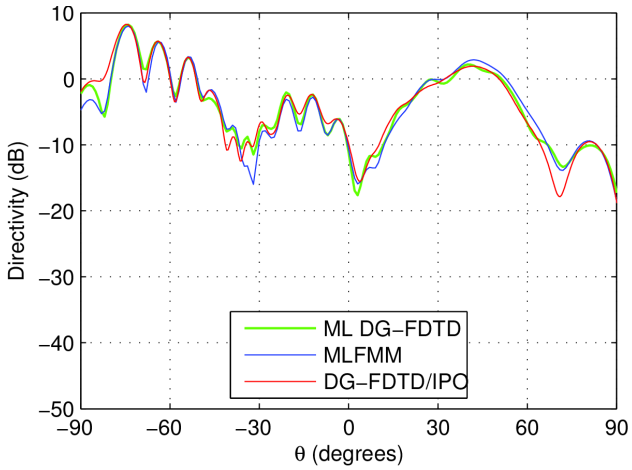

Fig. 7. E_θ far-field (CO-polar) in the (x0z) plane at 1GHz for the validation scenario.

FDTD $\lambda_{1GHz}/30$ mesh (volume size : $60 \times 80 \times 40$ unit cells). Finally, the third step takes into account the influence of the metallic structure using a $\lambda_{1GHz}/10$ cubic mesh (FDTD volume size : $170 \times 170 \times 65$ unit cells).

Radiation patterns computed by MLFMM and multi-level DG-FDTD are presented in Fig. 7 and Fig. 8. The reference results obtained with the two full wave multi-scale methods agree.

C. DG-FDTD/IPO simulation of the validation scenario

1) Decomposition of the EM problem: The DG-FDTD/IPO simulation of the validation scenario is based on two successive simulations (Fig. 6). First, the DG-FDTD method is used to analyze the domain including the monopole and the dielectric block. This DG-FDTD simulation is performed in two steps: the monopole lying on an infinite ground plane is first simulated using a fine ($\lambda_{1GHz}/60$) cubic mesh. Then, this monopole is computed in the presence of the dielectric material using a coarser FDTD mesh ($\lambda_{1GHz}/30$). In this second step, the antenna and the dielectric are both placed on an infinite ground plane. Once the DG-FDTD simulation has been completed, an IPO simulation is launched in order to take into account the influence of the metallic structure on the antenna radiation. This simulation uses a coarse ($\lambda_{1GHz}/6$) mesh, which results in a structure with $7,878$ facets. As indicated in section II, the antenna and the dielectric block are not described in this simulation.

It is worth noting that in the DG-FDTD/IPO simulation, the two DG-FDTD steps are the same as the first two steps in the ML DG-FDTD reference simulation (Fig. 5). Moreover, IPO simulation substitutes to the third step of the ML DG-FDTD.

2) Numerical results: The results presented in this section were computed with one IPO iteration ($N = 1$). A parametric study of the IPO iteration number has shown that far-field results reach a good convergence with only one iteration. However, as it is not within the scope of this article, the study is not presented here.

In order to quantify the accuracy of DG-FDTD/IPO, the radiated field is compared with the MLFMM results by evaluating the normalised mean absolute error ϵ given by

$$\epsilon = \frac{\sum_{i=1}^{N_\theta} |X(\theta_i) - X_{ref}(\theta_i)|}{N_\theta |\max_i [X_{ref}(\theta_i)]|} \quad (6)$$

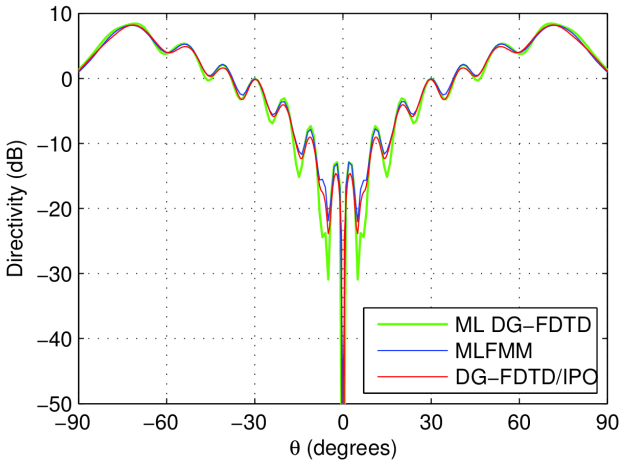

(a) E_θ (co-polar)

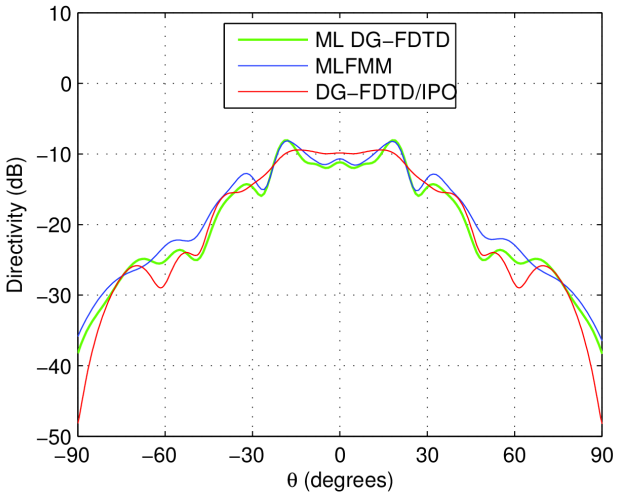

(b) E_ϕ (cross-polar)

Fig. 8. Far-field in the (y0z) plane at 1GHz for the validation scenario.

TABLE I
ERROR ϵ (%) ON THE FAR-FIELD COMPONENTS

	(x0z) plane	(y0z) plane	
	E_θ	E_θ	E_ϕ
MLFMM	-	-	-
ML DG-FDTD	1.77	2.20	3.53
DG-FDTD/IPO	2.51	1.56	5.97

TABLE II
COMPUTATION TIME ASSOCIATED WITH THE VALIDATION TEST CASE

	1 GHz	**[0.8 ; 1] GHz**
		(11 points)
ML DG-FDTD	3h 6 min	**3h 7 min**
MLFMM (FEKO)	24 min	**4h 28 min**
DG-FDTD/IPO	14 min	**21 min**

where X is either the E_θ (co-polar) or the E_ϕ (cross-polar) far-field complex component, $\theta_i = (-90 + (i-1))$ degrees, and $N_\theta = 181$. Subscript ref denotes the reference fields (MLFMM solution). ML DG-FDTD is also compared to MLFMM in order to better estimate the loss of accuracy involved by the IPO simulation (indeed, ML DG-FDTD and DG-FDTD/IPO only differ in this IPO simulation). All the results are presented in Table I.

It shows that the results coming from DG-FDTD/IPO are almost as accurate as the ones coming from ML DG-FDTD when compared with the reference far-field (MLFMM). Indeed, in the (x0z) plane, an error of 2.51% is observed with DG-FDTD/IPO compared to 1.77% with ML DG-FDTD. In the (y0z) plane, DG-FDTD/IPO gives even more accurate results than ML DG-FDTD (1.56% against 2.20%) for the co-polar component. However, the hybrid method presents a slight loss of accuracy for the cross-polar in this plane (5.97% against 3.53%). This can be explained by the fact that edge and wedge diffractions, which strongly determine the cross-polar radiated field, are not taken into account in the IPO simulation.

Fig. 7 and Fig. 8a present the E_θ (co-polar) far-field radiation pattern computed by DG-FDTD/IPO, and the reference methods in the (x0z) and (y0z) planes. These figures show that the DG-FDTD/IPO results are in very good agreement with those obtained by the two reference methods. Fig. 8b shows the E_ϕ (cross-polar) far-field radiation pattern in the (y0z) plane. Once again, results are in good agreement. It is worth noting that the simulation of the surrounded monopole gives a radiation pattern quite different from that of a monopole over an infinite ground plane. In particular, the traditional monopole radiation pattern does not show oscillations as in Fig. 8a or a cross polarisation component as in Fig. 8b.

So, these results indicate that the DG-FDTD/IPO method is capable of performing a reliable computation of the co- and the cross-polarisation components radiated by a surrounded antenna mounted on a metallic structure.

3) Computation time: Table II presents the computation time required by the new hybrid approach and the two reference methods. It must be noted that none of the three simulations compared here were performed using a parallelization scheme.

The left column refers to the computation of one frequency point (at 1 GHz), whereas the right column considers the computation of 11 frequency points taken over the [0.8;1]GHz band. First, DG-FDTD/IPO turns out to be faster than the reference methods in the two frequency configurations. In particular, it proves to be very efficient for the computation of 11 frequency points. This result indicates that the new hybrid method makes good use of the wide-band characteristic of DG-FDTD and the rapidity of IPO computation.

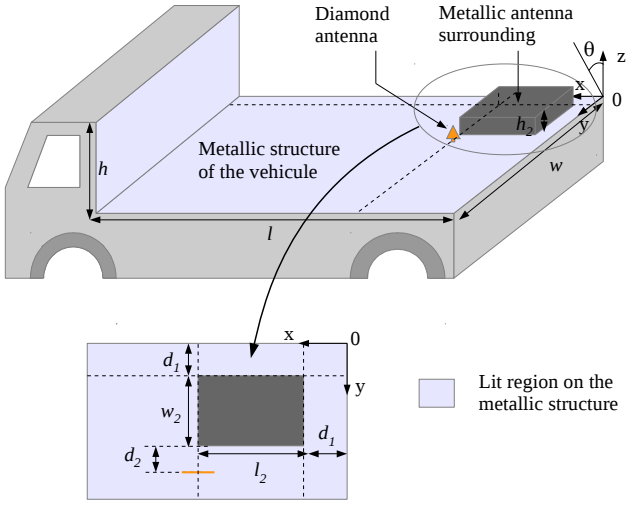

Fig. 9. Wide-band antenna and its vicinity mounted on a vehicle. l = 1728 mm; w = 1584 mm; h = 1008 mm; l_2 = 246 mm; w_2 = 168 mm; h_2 = 144 mm; d_1 = 78 mm; d_2 = 25.2 mm.

IV. APPLICATION OF DG-FDTD/IPO

In section III, the DG-FDTD/IPO method was validated for a canonical case. The aim of this section is to demonstrate its ability to analyze more realistic situations.

A. Description of the EM problem

A description of the studied problem is given in Fig. 9. A wide-band diamond antenna, identical to the one described in [9], is mounted on a metallic structure representing a vehicle. The antenna presents a reflection coefficient below -10 dB over the [5 ; 9.5] GHz band. A metallic box that could contain its electronic system (metallic parallelepiped) is placed close to the antenna. Considering its electrical dimensions (7.8 λ_0 × 5.3 λ_0 × 4.56 λ_0 at 9.5 GHz), this element may already be seen as an electrically large element. Finally, the dimensions (55 λ_0 × 50 λ_0 × 32 λ_0 at 9.5 GHz) of the metallic structure provide a highly multi-scale feature to this scenario, and they may be considered to be representative of a terrestrial drone. Note that the structure considered in the IPO simulation only corresponds to the top side of the platform (light blue part in Fig. 9) because of the visibility considerations in equations (1) and (3).

TABLE III
ERROR ϵ (%) ON THE FAR-FIELD

	(x0z) plane		(y0z) plane	
	E_θ	E_ϕ	E_θ	E_ϕ
MLFMM	-	-	-	-
DG-FDTD/IPO	5.93	14.37	0.825	7.60

TABLE IV
COMPUTATION TIME ASSOCIATED WITH THE EXPLOITATION TEST CASE

	radiation pattern at 9.5 GHz	wide-band computation (3.5 GHz bandwidth; 100 MHz step)
MLFMM (FEKO)	**7h 55 min**	**11 days**
DG-FDTD/IPO	**3h 19 min** DG-FDTD: 2h 56 min IPO: 23 min	**13h 44 min** DG-FDTD: 2h 56 min IPO: 10h 48min

The DG-FDTD/IPO computation of this EM problem is based on the breakdown proposed in Fig. 3 (section II). Hence, The initial EM problem is split into two simulations. First, DG-FDTD is used to simulate the diamond antenna, taking into account the metallic element in the vicinity. In the first step of DG-FDTD, the antenna is analyzed alone on an infinite ground plane. This simulation uses a very fine FDTD mesh ($\lambda_{9.5GHz}/105$) so as to correctly model the triangular geometry of the antenna and in so doing recover the measured performances as presented in [9]. Then, an FDTD simulation of the antenna with the metallic element in its vicinity is performed. A coarser mesh ($\lambda_{9.5GHz}/26.25$) is used during this step to reduce the computational resources. Note that the spatial discretization used in this second step of the DG-FDTD must both be a multiple of the one used in the first step ($\times 4$), and comply with the classic FDTD dispersion criteria. The DG-FDTD simulation is followed by an IPO simulation of the metallic structure hosting the antenna. The structure is discretized with $\lambda_{9.5GHz}/4.4$ square facets, about 19 facets per square wavelength. This sampling density is in agreement with the recommendation given in [24]. Finally, note that to compute the structure only one iteration is used in the IPO code.

B. Numerical results

The comparison of the radiation patterns computed with DG-FDTD/IPO and FEKO at 9.5 GHz is first presented. Then, the results of a wide-band computation are proposed.

1) comparison with FEKO at 9.5 GHz: Fig. 10 shows the radiation patterns computed with DG-FDTD/IPO and FEKO software at 9.5 GHz. To generate the FEKO results, the overall structure is simulated with the MLFMM method. The computation, on a 48 Gbit RAM workstation, requires an appropriate parametrization of the FEKO simulation. First, an SPAI (SParse Approximate Inverse) iterative preconditioner is used to reduce the memory. Moreover, the overall structure is discretized using a coarse mesh ($\lambda_{9.5GHz}/8$) with the exception of the antenna which is meshed more finely ($\lambda_{9.5GHz}/20$). So, the structure to be studied contains 1,324,360 triangles.

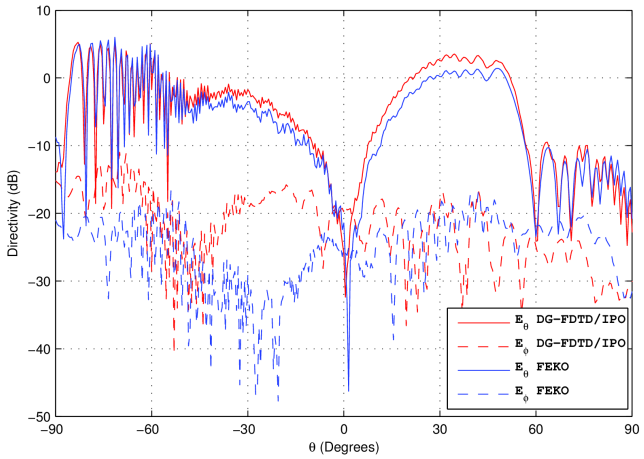

(a)

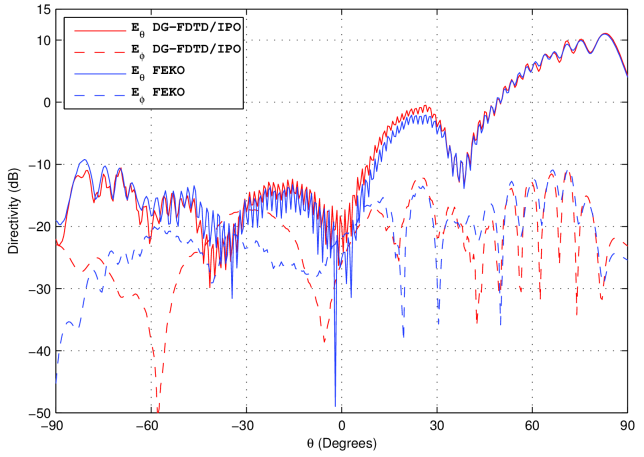

(b)

Fig. 10. Far-field at 9.5GHz with DG-FDTD/IPO and MLFMM (FEKO) in the (x0z) and the (y0z) planes, Fig. 10a and Fig. 10b respectively .

The error criteria given in equation 6 is used again to evaluate the accuracy of the DG-FDTD/IPO taking the MLFMM as reference. Note that the angular increment is reduced (here $N_{theta} = 361$) in order to follow the quick oscillations encountered at this frequency. The error ϵ on the E_θ and E_ϕ far-field components (respectively the co-polar and cross-polar) is presented in Table III.

The E_θ (co-polar) results (solid line in Fig. 10a and Fig. 10b) show a good agreement, especially in the (y0z) plane. Indeed, an error of 5.93% is observed with the hybrid method in the (x0z) plane. This error is even reduced to 0.825% in the (y0z) plane. This demonstrates that the new hybrid approach is capable of accurately computing large and highly multi-scale problems.

Two reasons may be put forward to explain the differences on the cross-polar component. First, the antenna vicinity is not redescribed in the IPO simulation. Then, it is well known that the classic (I)PO method does not take into account the

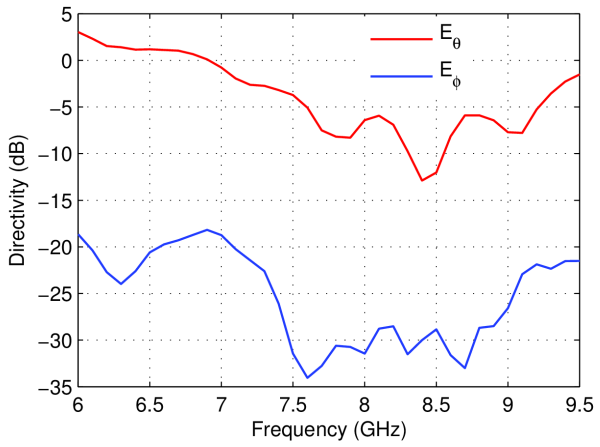

Fig. 11. Computation of the electric far field for θ = + 45 degrees in the (y0z) plane over the [6 ; 9.5] GHz band.

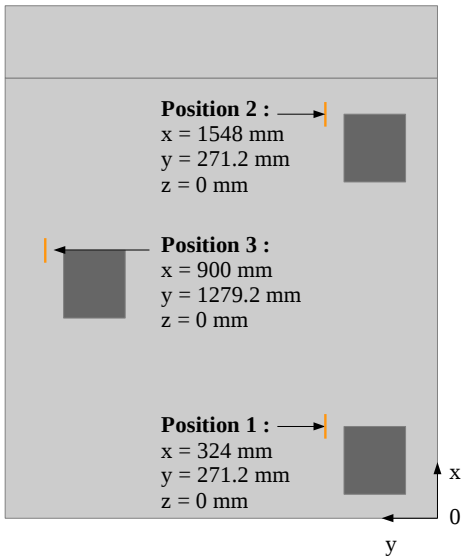

Fig. 12. Antenna placement : three positions studied for the antenna and its vicinity on the vehicle (top side view).

edge/wedge diffractions. But these diffractions may have a significant effect on the cross-polar component.

Finally, as can be seen from Table IV, time-saving provided by DG-FDTD/IPO is very significant for such realistic problems.

2) Wide-band computation: One of the benefits of the DG-FDTD/IPO method is its wide-band characteristic. In order to illustrate this aspect a wide-band computation was performed. As an example, the electric far-field in the (y0z) plane for θ = 45 degrees over the [6 ; 9.5] GHz band is shown in Fig. 11. Note that a 100 MHz step was used.

Table IV also presents the computation time associated with the simulation of the far-field over the 3.5 GHz bandwidth with DG-FDTD/IPO and MLFMM (FEKO). These results clearly show the efficiency of DG-FDTD/IPO to compute wide-band parameters. Indeed, the wider the analysis bandwith used, the more attractive the DG-FDTD/IPO method becomes. As indicated in section III-C3, the wide-band efficiency of the new hybrid method is both linked to the wide-band characteristic of the DG-FDTD and the low computational cost required by the IPO simulation.

3) Antenna placement: We have seen before that DG-FDTD/IPO could provide an efficient way to accurately simulate surrounded antennas mounted on electrically large structures. This hybrid approach may also be very useful to quickly optimize antenna placement. Indeed, the DG-FDTD/IPO method allows the simulation to be performed for several positions without computing the overall problem for each position. In order to illustrate this point, the simulation of the diamond antenna and the metallic box, including its electronic system, was carried out for three different positions on the structure (Fig. 12). The results of these three simulations are presented in Fig. 13.

In table IV, the computation time needed to perform those three simulations with the DG-FDTD/IPO approach is compared to the one required to perform the same simulations with MLFMM (FEKO). It shows that the DG-FDTD/IPO approach greatly reduces the computation time associated with the simulation of antenna in different positions on the structure. This is mainly due to the fact that the DG-FDTD/IPO approach can reuse the simulation of the monopole in the presence of the metallic scatterer. So, once the antenna and its complex surrounding environment have been simulated (DG-FDTD), only IPO simulation has to be repeated to compute the radiation patterns associated with a new position.

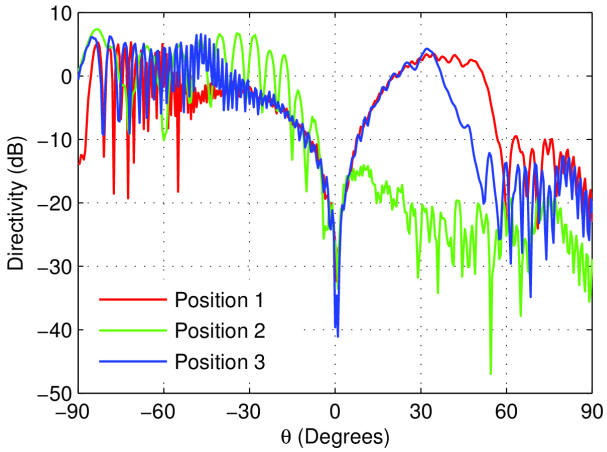

Fig. 13. E_θ Radiation pattern in the (x0z) plane for three positions.

V. Conclusion

A new hybrid approach associating DG-FDTD and IPO is proposed. This method, called DG-FDTD/IPO, allows accurate and efficient simulation of wide-band surrounded antennas mounted on large metallic platforms.

This approach was first validated on a canonical test case by comparison with two multi-scale reference methods (MLFMM and ML DG-FDTD). The rapidity and the accuracy of the proposed method are shown. The new hybrid method was next used to analyze a real-life problem regarding a wide-band

TABLE V
COMPUTATION TIME ASSOCIATED WITH THE OPTIMIZATION OF THE ANTENNA PLACEMENT

	Computation of 1 position	Computation of the 3 positions
MLFMM (FEKO)	**7h 55 min**	**23h 45 min**
DG-FDTD/IPO	**3h 19 min**	**4h 06 min**
	-DG-FDTD: 2h 56 min	-DG-FDTD: 2h 56 min
	-IPO: 23 min	-IPO: 1h 10 min

antenna mounted on a vehicle. Comparisons with MLFMM computations performed on FEKO show a good agreement. Finally, the new approach proved to be faster than the commercial code, especially for the computation of wide-band parameters, and the optimization of antenna placement.

ACKNOWLEDGMENT

This work was supported by the French Defense Agency (Direction Générale de l'Armement, DGA) and the French Space Agency (Centre National des Etudes Spatiales, CNES). The authors thank Mr J. Burdon for its valuable help during the proofreading of this paper.

REFERENCES

[1] J. F. Zhang, X. Wei Ping, W. M. Yu, X. Y. Zhou, and T. J. Cui, "Space antenna modeling," in *Space Antenna Handbook*. John Wiley and Sons, Ltd, may 2012, ch. 2, pp. 36–75.

[2] J.-Z. Lei, C.-H. Liang, W. Ding, and Y. Zhang, "EMC analysis of antennas mounted on electrically large platforms with parallel FDTD method," *Prog. Electromagn. Res.*, vol. 84, pp. 205–220, 2008.

[3] D. J. Riley, M. F. Pasik, J. D. Kotulski, C. D. Turner, and N. W. Riley, "Analysis of airframe-mounted antennas using parallel and hybridized finite-element time-domain methods," in *IEEE Antennas Propag. Soc. Int. Symp.*, vol. 3, 2002, pp. 168–171.

[4] A. Barka and P. Caudrillier, "Domain decomposition method based on generalized scattering matrix for installed performance of antennas on aircraft," *IEEE Trans. Antennas Propag.*, vol. 55, no. 6, pp. 1833–1842, Jun. 2007.

[5] X. Wang, Z. Peng, K.-H. Lim, and J.-F. Lee, "Multisolver domain decomposition method for modeling EMC effects of multiple antennas on a large air platform," *IEEE Trans. Electromagn. Compat.*, vol. 54, no. 2, pp. 375–388, Apr. 2012.

[6] J. M. Johnson and Y. Rahmat-Samil, "MR/FDTD: A multiple-region finite-difference–time-domain method," *Microw. Opt. Technol. Lett.*, vol. 14, no. 2, pp. 101–105, Feb. 1997.

[7] X.-W. Zhao, X.-J. Dang, Y. Zhang, and C.-H. Liang, "The multilevel fast multipole algorithm for EMC analysis of multiple antennas on electrically large platforms," *Prog. Electromagn. Res.*, vol. 69, pp. 161–176, 2007.

[8] U. Jakobus, J. Van Tonder, and M. Schoeman, "Advanced EMC modeling by means of a parallel MLFMM and coupling with network theory," in *Proc. IEEE Int. Symp. Electromagn. Compat.*, Aug. 2008, pp. 1–5.

[9] R. Pascaud, R. Gillard, R. Loison, J. Wiart, and M. F. Wong, "Dual-grid finite-difference time-domain scheme for the fast simulation of surrounded antennas," *IET Microw. Antennas Propag.*, vol. 1, no. 3, p. 700, 2007.

[10] P. H. Pathak, "High-frequency techniques for antenna analysis," *Proc. IEEE*, vol. 80, pp. 44–65, Jan. 1992.

[11] A. K. Bhattacharyya, *High-Frequency Electromagnetic Techniques : Recent Advances And Applications*. John Wiley and Sons, 1995.

[12] U. Jakobus and F. M. Landstorfer, "Improved PO-MM hybrid formulation for scattering from three-dimensional perfectly conducting bodies of arbitrary shape," *IEEE Trans. Antennas Propag.*, vol. 43, no. 2, pp. 162–169, Feb. 1995.

[13] R. Hodges and Y. Rahmat-Samii, "An iterative current-based hybrid method for complex structures," *IEEE Trans. Antennas Propag.*, vol. 45, no. 2, pp. 265–276, 1997.

[14] F. Obelleiro, J. M. Taboada, J. L. Rodríguez, J. O. Rubinos, and A. M. Arias, "Hybrid moment-method physical-optics formulation for modeling the electromagnetic behavior of on-board antennas," *Microw. Opt. Technol. Lett.*, vol. 27, pp. 88–93, 2000.

[15] Z.-L. Liu and C.-F. Wang, "Efficient iterative method of moments-physical optics hybrid technique for electrically large objects," *IEEE Trans. Antennas Propag.*, vol. 60, no. 7, pp. 3520–3525, Jul. 2012.

[16] T. Ozdemir, M. W. Nurnberger, J. L. Volakis, R. Kipp, and J. Berrie, "A hybridization of finite-element and high-frequency methods for pattern prediction for antennas on aircraft structures," *IEEE Antennas Propag. Mag.*, vol. 38, no. 3, pp. 28–38, Jun. 1996.

[17] R. Fernández-Recio, L. E. García-Castillo, I. Gómez-Revuelto, and M. Salazar-Palma, "Fully coupled multi-hybrid FEM-PO/PTD-UTD method for the analysis of radiation problems," *IEEE Trans. Magn.*, vol. 43, no. 4, pp. 1341–1344, Apr. 2007.

[18] F. Le Bolzer, R. Gillard, J. Citerne, V. F. Hanna, and M. F. Wong, "An hybrid formulation combining FDTD and TDPO," in *IEEE AP-S Int. Antennas Propag. Symp.*, vol. 2, Atlanta, USA, Jun. 1998, pp. 952–955.

[19] J. Lanoe, M. M. Ney, and S. Le Maguer, "Time-domain equivalent edge current (TD-EEC's) technique to improve a TLM-physical optics hybrid procedure," in *Proc. 2nd Eur. Antennas Propag. Conf.*, Edinburgh, UK, Nov. 2007, pp. 1–5.

[20] L.-X. Yang, D.-B. Ge, and B. Wei, "FDTD/TDPO hybrid approach for analysis of the EM scattering of combinative objects," *Progr. Electromagn. Res.*, vol. 76, pp. 275–284, 2007.

[21] A. Noga and T. Topa, "Efficient analysis of radiating problems by hybrid FDTD/PO method," in *Proc. 4th Eur. Antennas Propag. Conf.*, Barcelona, Spain, Apr. 2010, pp. 1–4.

[22] T.-T. Chia, R. Burkholder, and R. Lee, "The application of FDTD in hybrid methods for cavity scattering analysis," *IEEE Trans. Antennas Propag.*, vol. 43, no. 10, pp. 1082–1090, 1995.

[23] R. J. Burkholder, P. H. Pathak, K. Sertel, R. J. Marhefka, J. L. Volakis, and R. W. Kindt, "A hybrid framework for antenna/platform analysis," *Applied Computational Electromagn. Society Journal*, vol. 21, pp. 177–195, Nov. 2006.

[24] F. Obelleiro-Basteiro, J. Luis Rodriguez, and R. Burkholder, "An iterative physical optics approach for analyzing the electromagnetic scattering by large open-ended cavities," *IEEE Trans. Antennas Propag.*, vol. 43, no. 4, pp. 356–361, Apr. 1995.

[25] R. Burkholder and T. Lundin, "Forward-backward iterative physical optics algorithm for computing the RCS of open-ended cavities," *IEEE Trans. Antennas Propag.*, vol. 53, no. 2, pp. 793–799, Feb. 2005.

[26] R. Hémon, P. Pouliguen, H. He, J. Saillard, and J.-F. Damiens, "Computation of EM field scattered by an open-ended cavity and by a cavity under radome using the iterative physical optics," *Progr. Electrom. Res.*, vol. 80, pp. 77–105, 2008.

[27] J. Li, B. Wei, Q. He, L.-X. Guo, and D.-B. Ge, "Time-domain iterative physical optics method for analysis of EM scattering from the target half burried in rough surface: Pec case," *Progr. Electrom. Res.*, vol. 121, pp. 391–408, 2011.

[28] R. Burkholder, "A fast and rapidely convergent iterative physical optics algorithm for computing the RCS of open-ended cavities," *Appl. Computational. Electromagn. Soc. J.*, vol. 16, no. 1, pp. 53–60, March. 2001.

[29] F. Obelleiro, M. G. Araujo, and J. L. Rodríguez, "Iterative physical-optics formulation for analyzing large waveguides with lossy wall," *Microw. Opt. Technol. Lett.*, vol. 28, no. 1, pp. 21–26, Jan. 2001.

[30] R. Pascaud, R. Gillard, R. Loison, L. Le Coq, J. Thevenard, A. Louzir, D. L. H. Tong, C. Nicolas, C. Person, and J. P. Coupez, "Numerical modeling of an integrated multi-sector antenna using the DG-FDTD method," in *Eur. Microw. Conf. (EuMC)*, Rome, Italy, Sep. 2009, pp. 850–853.

[31] J.-M. Jin, "Electromagnetic theorems and principles," in *Theory and Computation of electromagnetic fields*. John Wiley and Sons, Inc., 2010, ch. 3, pp. 87–90.

[32] R. J. Burkholder, C. Tokgoz, C. J. Reddy, and P. H. Pathak, "Iterative physical optics: it's not just for cavities anymore," in *IEEE AP-S Int. Antennas Propag. Symp.*, vol. 1A, Jul. 2005, pp. 18–21.

[33] C. Miry, R. Gillard, and R. Loison, "Multi-level dual-grid finite-difference time-domain approach for the analysis of body implanted antennas," *IET Microw. Antennas Propag.*, vol. 4, no. 6, p. 659, 2010.

[34] FEKO (www.feko.info) 6.2, EM Software and Systems - S.A. (Pty) Ltd, 32 Techno Avenue, Technopark, Stellenbosch, 7600, South Africa.

Benoit Le Lepvrier was born in Pabu, France, in 1988. He received the Diplôme d'Ingénieur (Master level) degree in network and communication systems from the National Institute of Applied Sciences (INSA), Rennes, France, in 2011. He is currently working toward the Ph.D. degree in electronics at the Electronics and Telecommunications Institute of Rennes (IETR), France (in collaboration with the Centre National d'Etudes Spatiales (CNES), Toulouse, France and the Direction Générale de l'Armement (DGA) Bruz, France). His research interests are computational electromagnetics for antennas on electrically large and complex platforms.

Renaud Loison was born in Saint-Brieuc, France, on January 16, 1974. He received the Diplôme d'Ingénieur and Ph.D. degrees from the National Institute of Applied Sciences (INSA), Rennes, France, in 1996 and 2000, respectively. In 2000, he joined the Institute of Electronics and Telecommunications of Rennes (IETR), Rennes, France, as an Associate Professor. Since 2009, he has been a Professor with the Complex Radiating Systems Group, IETR. His research interests concern reflectarrays and numerical methods applied to the computer-aided design (CAD) and optimization of microwave circuits and antennas.

Raphaël Gillard received the Ph.D. degree in electronics from the National Institute of Applied Sciences (INSA), Rennes, France, in 1992. He initially worked as a Research Engineer with the IPSIS Company, Cesson-Sévigné, France, where he developed a commercial method of moments (MoM) code for the simulation of microwave circuits and antennas. In 1993, he joined the National Institute of Applied Sciences (INSA), Rennes, France, as an Assistant Professor. Since 2001, he has been a Full Professor with the Antenna and Microwave Group, Electronics and Telecommunications Institute of Rennes (IETR), Rennes, France, where he was in charge of electromagnetic (EM) modeling and optimization activity. Since 2006, he has been leading the Antenna and Microwave Group. He has coauthored 164 conference papers and 62 journal papers. His current main research interests are computational electromagnetics and reflectarrays. Prof. Gillard was a member of both the Executive and Governing Boards of the European Antenna Centre of Excellence (ACE) from 2004 to 2008. He was co-leader of its antenna software activity (in charge of the software benchmarking work package). He is member of several scientific committees or review boards (EuCAP, EuMC, etc.).

Laurent Patier was born in Vichy, France, in 1984. He obtained his Master's degree in Electromagnetic Compatibility and in Opto/Micro-Electronics in 2007 at the University of Clermont-Ferrand (France). He received the Ph.D. degree in 2010 at ONERA (Toulouse, France). In 2010, he joined the French Space Agency (CNES, Toulouse, France) as an engineer in antenna modelling. Since 2013, he has been working in the EMC lab in the department "board electrical equipments" at CNES.

Philippe Pouliguen received the M.S. degree in signal processing and telecommunications, the Doctoral degree in electronic and the "Habilitation à Diriger des Recherches" degree from the University of Rennes 1, France, in 1986, 1990 and 2000. In 1990, he joined the Direction Générale de l'Armement (DGA) at the Centre d'Electronique de l'Armement (CELAR), now DGA Information Superiority (DGA/IS), in Bruz, France, where he was a "DGA expert" in electromagnetic radiation and radar signatures analysis. He was also in charge of the EMC (Expertise and ElectoMagnetism Computation) laboratory of CELAR. Since December 2009, he has been the head of "acoustic and radio-electric waves" scientific domain at the office for advanced research and innovation of the strategy directorate, DGA, Bagneux, France. His research interests include electromagnetic scattering and diffraction, Radar Cross Section (RCS) measurement and modeling, asymptotic high frequency methods, radar signal processing and analysis, antenna scattering problems and Electronic Band Gap Materials. In these fields, he has published more than 30 articles in refereed journals and more than 100 conference papers.